Utrecht University

Topology of Weyl semimetals
with non-orientable Brillouin zones

by

Thijs Douwes

A thesis

Submitted to the Department of Physics
in partial fulfilment of the requirements
for the degree of

Master of Science

under the joint supervision of

Project supervisor
Prof. Cristiane de Morais Smith
Department of Physics

Direct supervisor
Dr. Marcus Ståhammar
Department of Physics

October 2024

Abstract

Contents

Chapter 1

Introduction

Example citation.[Fon+24] Example expanded citation.[MT17, Remark 3.8]

1.1 Main results

1.2 Overview

1.3 Prerequisites

1.4 Notational conventions

Chapter 2

Topological states of matter & symmetries

Sources: [Akh+; AOP16; BH13; SA17]
Topo phases occur in nature: [Geh+13]
Finish intro when chapter is more complete

2.1 Basic definitions

- Conducting properties of materials are understood in terms of band structure → Fermi energy. Conductance means Fermi level lies inside one of the bands. [picture]
- N-band system has hilbert space $\mathcal{H} \cong \mathbb{C}^N$, Hamiltonian represented by $N \times N$ matrix. Static system: $H\psi = E\psi$, eigenvalues are energy bands.
- Mostly interested in 2-band systems since only valence/conduction bands are relevant. Then H is a 2×2 Hermitian (for now) matrix. These are given by $H = h_0\mathbb{I} + \mathbf{h} \cdot \boldsymbol{\sigma}$ in general (h_0 changes the energy of all bands but does not affect topology of band crossings) → Bloch Hamiltonian [higher dimensional systems: Clifford algebra]
- For a Bloch Hamiltonian, eigenvalues are $\pm|\mathbf{h}|$, so conductance occurs when $\mathbf{h} = 0$.
- Insulating Hamiltonians are adiabatically connected if they can be continuously deformed into each other without band crossings. Insulators are considered topological if they are not adiabatically connected to a reference trivial phase; then these inhabit different regions of the phase diagram → existence of edge states (not always [BH13], footnote)

2.1.1 Bloch theory

- We work with crystalline materials which are composed of periodically repeating unit cells.
- In the bulk, we assume the Hamiltonian is periodic in the unit cell. This enables use of Bloch's theorem [Blo29] $\psi(\mathbf{r}) = \mathrm{e}^{i\mathbf{k}\cdot\mathbf{r}}\, u_{\mathbf{k}}(\mathbf{r})$.
- Different values of crystal momentum may yield identical eigenstates, the set of equivalence classes is the Brillouin zone
- Brillouin zone usually has $\mathbb{T}^n$ topology, but internal symmetries etc. may alter this [Fon+24] [other sources]
- Discuss dispersion relations

2.2 The Su–Schrieffer–Heeger model

- SSH is usually introduced "physics first", but we would like to work backwards in a sense, to see how bulk topology gives rise to physical properties of a system.

We will take the approach of deriving the Su–Schrieffer–Heeger (SSH) model by beginning with a generic one-dimensional crystal, and introducing two topologically distinct phases in the simplest way possible.

Concretely, consider an infinite one-dimensional chain of unit cells indexed by $n \in \mathbb{Z}$; at this point, we make no assumptions on the internal structure of these unit cells. A boundary will be introduced later, but its relevant properties will turn out to be determined by the crystal's bulk topology. Suppose the real-space Hamiltonian of the system is periodic in the unit cells. By Bloch's theorem, two crystal momenta k and k' are then equivalent if they differ by an integer multiple of 2π. This means that the Brillouin zone B can be taken to be the interval $[-\pi, \pi]$, with the points $-\pi$ and π identified; this space is homeomorphic to the circle S^1.

We might begin with a simple two-band Bloch Hamiltonian $H(k) = \mathbf{h}(k) \cdot \boldsymbol{\sigma}$, with

$$\mathbf{h} : B \cong S^1 \to \mathbb{R}^3, \quad k \mapsto \begin{pmatrix} h_x(k) \\ h_y(k) \\ h_z(k) \end{pmatrix}.$$

Such a Hamiltonian describes a gapped phase precisely when the map $\mathbf{h}$ is non-zero everywhere, so that the topological classification of these phases is given by classes of maps from S^1 to $\mathbb{R}^3$ minus the origin—that is, homotopy classes of loops in $\mathbb{R}^3 \setminus \{0\}$. However, this space has a trivial fundamental group $\pi_1\big(\mathbb{R}^3 \setminus \{0\}\big) \cong 0$, meaning that all such loops can be contracted to a point; in other words, all gapped Hamiltonians are adiabatically connected, and there are no topologically interesting phases.

This situation can be remedied by imposing a constraint on the Hamiltonian: we require that $h_z(k) = 0$. Doing this effectively reduces $\mathbf{h}$ to a two-dimensional map:

$$\mathbf{h} : B \cong S^1 \to \mathbb{R}^3, \quad k \mapsto \begin{pmatrix} h_x(k) \\ h_y(k) \end{pmatrix}.$$

The gapped phases are now classified by the non-trivial fundamental group $\pi_1\big(\mathbb{R}^2 \backslash \{\, 0 \,\}\big) \cong \mathbb{Z}$. This group is indexed by winding number: loops that wind around the origin $a \in \mathbb{Z}$ times cannot be deformed into those with a different winding number $b \neq a$. In particular, loops with a non-zero winding number cannot be contracted to a point, and the associated phases are considered topological. Note that imposing a constraint on the Hamiltonian has made this system rather more interesting from a topological point of view, even though it seems like we have simplified it. Once we move to the physical picture, we will see that this restriction corresponds to imposing a certain symmetry on the system.

Let us now choose a more specific Hamiltonian to arrive at a concrete physical system. We begin with the simplest possible* topologically distinct states, one trivial and one topological:

$$\mathbf{h}_{\text{triv}}(k) = \begin{pmatrix} 1 \\ 0 \\ 0 \end{pmatrix}, \qquad \mathbf{h}_{\text{top}}(k) = \begin{pmatrix} \cos(k) \\ \sin(k) \\ 0 \end{pmatrix}.$$

To characterise a phase transition between these two states, we consider the linear combination $\mathbf{h}(k) = v\mathbf{h}_{\text{triv}}(k) + w\mathbf{h}_{\text{top}}(k)$, with $v, w \geq 0$. The phase described by the resulting Bloch Hamiltonian is trivial when $v > w$, gapless (i.e. conducting) when $v = w$, and topological when $v < w$; see Figure 2.1.

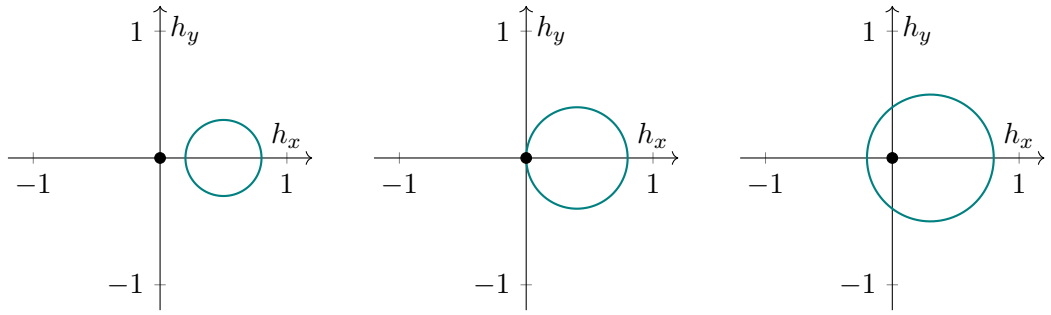

(a) $v = 0.5$, $w = 0.3$ (b) $v = w = 0.4$ (c) $v = 0.3$, $w = 0.5$

Figure 2.1: Contours in Hamiltonian space for (a) trivial, (b) conducting and (c) topological phases.

We are now in a position to start analysing the physics of the system. Concretely, the momentum space Hamiltonian is given by

$$H(k) = \mathbf{h}(k) \cdot \boldsymbol{\sigma} = \big(v + w\cos(k)\big)\sigma_x + w\sin(k)\sigma_y = \begin{pmatrix} 0 & v + w\,\mathrm{e}^{-ik} \\ v + w\,\mathrm{e}^{ik} & 0 \end{pmatrix}.$$

*Our particular choice of x, y, and z coordinates very conveniently leads to the SSH model. However, mathematically speaking, all similar models are related by a simple change of basis.

We can set up a Fourier transform to real space by rewriting this suggestively in terms of the unit cell index n:

$$H(k) = \mathrm{e}^{-ik(n-n)} \begin{pmatrix} 0 & v \\ v & 0 \end{pmatrix} + \mathrm{e}^{-ik\big((n+1)-n\big)} \begin{pmatrix} 0 & w \\ 0 & 0 \end{pmatrix} + \mathrm{e}^{-ik\big(n-(n+1)\big)} \begin{pmatrix} 0 & 0 \\ w & 0 \end{pmatrix}$$

I need to work out the details of this Fourier transform later, my calculations aren't working out. Transforming from a periodic Brillouin zone to (discrete or infinite) real space is breaking my brain. I imagine it needs to look something like this (where $M_{0/\pm1}$ are the three matrices above):

$$\begin{aligned}
\hat{H} &= \int_B H(k) \left|k\right\rangle \left\langle k\right| \\
&= \int_{-\pi}^{\pi} \frac{\mathrm{d}k}{2\pi} \left(\sum_{a\in\{0,\pm1\}} \mathrm{e}^{-ika} M_a \right) \left(\sum_n \mathrm{e}^{-ikn} \left|n\right\rangle \right) \left(\sum_{n'} \left\langle n'\right| \mathrm{e}^{ikn'} \right) \\
&= \sum_{a,n,n'} \left(\int_{-\pi}^{\pi} \frac{\mathrm{d}k}{2\pi} \mathrm{e}^{-ik(a+n-n')} \right) M_a \left|n\right\rangle \left\langle n'\right| \\
&= \sum_{a,n,n'} \delta_{n+a,n'} M_a \left|n\right\rangle \left\langle n'\right| \\
&= \sum_{a,n} M_a \left|n\right\rangle \left\langle n+a\right|
\end{aligned}$$

But I don't fully understand the first step, the sign of a is wrong and normalization is broken. Maybe it's easier to discretize first and do a DFT?

- It follows [how exactly?] that we can write the Hamiltonian in a unit cell basis as

$$\hat{H} = \sum_{n=-\infty}^{\infty} \left[\left|n\right\rangle \left\langle n\right| \otimes \begin{pmatrix} 0 & v \\ v & 0 \end{pmatrix} + \left(\left|n+1\right\rangle \left\langle n\right| \otimes \begin{pmatrix} 0 & w \\ 0 & 0 \end{pmatrix} + \text{h.c.} \right) \right]$$

- Mention tight binding somewhere around this point

This Hamiltonian contains a term which acts within the unit cells, and terms which act between neighbouring unit cells, parametrized by v and w respectively. The structure of these interactions can be made somewhat more transparent by going to a finite chain of length N. The Hamiltonian then becomes

$$\hat{H} = \sum_{n=0}^{N} \left|n\right\rangle \left\langle n\right| \otimes \begin{pmatrix} 0 & v \\ v & 0 \end{pmatrix} + \sum_{n=0}^{N-1} \left(\left|n+1\right\rangle \left\langle n\right| \otimes \begin{pmatrix} 0 & w \\ 0 & 0 \end{pmatrix} + \text{h.c.} \right),$$

where we have introduced open boundary conditions on the ends of the chain. This will allow us to study the boundary behaviour momentarily. We can then expand the tensor

products in order to cast the Hamiltonian into a full $2N \times 2N$ matrix:

$$\hat{H} = \begin{pmatrix} 0 & v & 0 & 0 & & & & \\ v & 0 & w & 0 & & & & \\ 0 & w & 0 & v & & & & \\ 0 & 0 & v & 0 & & & & \\ & & & & \ddots & & & \\ & & & & & 0 & 0 & \\ & & & & & w & 0 & \\ & & & & & 0 & w & 0 & v \\ & & & & & 0 & 0 & v & 0 \end{pmatrix}.$$

A physical interpretation of this system presents itself in the form of this matrix: it describes a chain of $2N$ sites, with alternating hopping amplitudes v and w between neighbouring sites. The unit cells now consist of two of these sites, and v and w are referred to as the *intra-cell* and *inter-cell* hoppings, respectively. When these two hoppings are equal we are in the gapless phase $v = w$, corresponding to a chain where all bonds are equally strong. Intuitively, this homogeneity allows electrons to propagate freely along the chain. On the other hand, in the insulating cases $v \neq w$, one of the two hoppings is stronger than the other, and the electrons tend to be confined around these stronger bonds.

Dividing the unit cells into two individual sites in this way allows us to distinguish two so-called *sublattices* of the crystal, which we label A and B. The notation can then be simplified by labelling quantum states according to the sublattice on which they are localized:

$$|n, A\rangle \equiv |n\rangle \otimes \begin{pmatrix} 1 \\ 0 \end{pmatrix}, \quad |n, B\rangle \equiv |n\rangle \otimes \begin{pmatrix} 0 \\ 1 \end{pmatrix}.$$

In this notation, the Hamiltonian becomes

$$\hat{H} = \left(\sum_{n=0}^{N} v \, |n, B\rangle \langle n, A| + \sum_{n=0}^{N-1} w \, |n+1, A\rangle \langle n, B| \right) + \text{h.c.} \tag{2.1}$$

The tight-binding model of alternating hoppings is precisely the SSH model: it was introduced in 1979 by Wu-Pei Su, John Robert Schrieffer, and Alan J. Heeger to describe polyacetylene (Figure 2.2), a polymer chain which features alternating single and double covalent bonds [SSH79; SSH80]. This material displays unexpectedly high conductivity when doped with halogen impurities, and the SSH model affords an explanation for this.

To understand how this metallic behaviour comes about, we need to examine the differences between the trivial and the topological phase more closely. The two phases appear to be identical at a first glance: if we choose the unit cell in polyacetylene in such a way that the stronger double bond represents the intra-cell hopping v, then we are in the trivial phase $v > w$, and if we centre the unit cell around a single bond, we have $v < w$ and the phase is topological. In either case, we expect valence electrons to remain

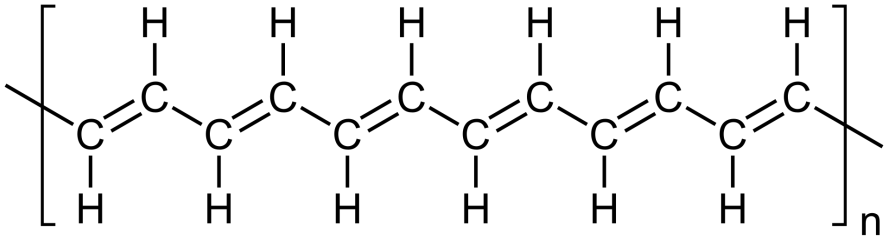

Figure 2.2: Structural diagram of polyacetylene. Electrons are transported more readily along the double bonds, which is modelled using a larger hopping parameter.

localized around the double bonds, leading to the same insulating bulk behaviour.[†]

The difference between the two phases only becomes apparent when we look at the endpoints of the chain. [introduce a figure here]For example, the leftmost atom is not subject to any inter-cell hopping, and it is only connected to the other atom in its unit cell. In the trivial case, this connection is strong and the two atoms share their valence electrons. In the topological phase, on the other hand, the second atom from the left prefers to share electrons with its right-hand neighbour, and the leftmost atom becomes isolated. In the limit where v goes to zero, this isolation becomes complete and the edge sites carry zero-energy eigenstates. In this case, only the second term in the Hamiltonian (2.1) survives, and the edges obey the eigenvalue equations

$$\hat{H}\,|1, A\rangle = \hat{H}\,|N, B\rangle = 0.$$

These edge modes can be shown to persist for non-zero $v < w$, in which case they become highly localized and approach zero energy in the $N \to \infty$ limit.[‡] The salient point is that the boundary modes of the topological phase are gapless: their energy eigenvalues have a degeneracy at the Fermi level $\varepsilon_F = 0$. [Perhaps include dispersion figure]

Something remarkable has happened: we have started from a topological description of a gapped bulk phase, and the resulting physical effects appear as gapless edge modes on the boundary of the material. As we will see, this is a fairly[§] general feature of topological phases of matter, called the *bulk-boundary correspondence*. We can think of it as being a result of the inability to go continuously from a topological gapped phase to a trivial one in real space; in particular, the outside boundary of an idealised material connects to the vacuum, which is also considered a trivial gapped phase.

[†]The attentive reader might wonder why the conducting $v = w$ phase does not occur naturally in this system. This is a result of the so-called Peierls transition: in a nutshell, introducing a band gap locally lowers the energy of the (filled) valence band and raises that of the (empty) conduction band. This makes it energetically favourable for atoms in the chain to pair up, in a process referred to as dimerisation.

[‡]A precise understanding of this is beyond the scope of this review; the interested reader is referred to e.g. [AOP16].

[§]This is not a completely general statement: topological phases with gapped edge modes have been shown to be theoretically feasible [Fre+04]. For our purposes, it will be sufficient to restrict our attention to the gapless edge modes.

- Discuss physics of polyacetylene (solitons on trivial/topological interface) and experimental observations of solitons + berry phase [MAG16; Ata+13]
- We can now physically interpret the meaning of setting $h_z = 0$: it ensures that hopping only occurs between the two sublattices A and B, and not within them (i.e. there are only off-diagonal elements in the internal degrees of freedom). If we define the sublattice projection operators

$$\hat{P}_A = \mathbb{I} \otimes \begin{pmatrix} 1 & 0 \\ 0 & 0 \end{pmatrix}, \quad \hat{P}_B = \mathbb{I} \otimes \begin{pmatrix} 0 & 0 \\ 0 & 1 \end{pmatrix}$$

  then the Hamiltonian obeys

$$\hat{P}_A \hat{H} \hat{P}_A = \hat{P}_B \hat{H} \hat{P}_B = 0$$

  and so since $\hat{P}_A + \hat{P}_B$ is the identity we have

$$\begin{aligned} \hat{H} &= (\hat{P}_A + \hat{P}_B)\hat{H}(\hat{P}_A + \hat{P}_B) \\ &= \hat{P}_A \hat{H} \hat{P}_B + \hat{P}_B \hat{H} \hat{P}_A \\ &= (\hat{P}_A - \hat{P}_B)\hat{H}(\hat{P}_B - \hat{P}_A) \\ &\equiv -\hat{\Gamma} \hat{H} \hat{\Gamma} \end{aligned}$$

  with $\hat{\Gamma} \equiv \hat{P}_A - \hat{P}_B$ having the property that $\hat{\Gamma} = \hat{\Gamma}^{-1} = \hat{\Gamma}\dagger$; this is called sublattice symmetry and it also applies to the momentum space Hamiltonian $H(k)$.
- An immediate consequence of our setup is that the trivial and topological phase become adiabatically connected if we allow for sublattice symmetry breaking ($h_z \neq 0$).
- Talk more about $\mathbb{Z}$ invariant (next-nearest-neighbour hopping etc.)

2.3 Two-dimensional models

2.3.1 Quantum Hall effect

2.3.2 The Chern insulator

2.3.3 The Kane–Mele model

2.4 Classification of symmetries

Chapter 3

Weyl semimetals

3.1 Physical aspects

3.2 Topological description

3.2.1 3D Chern insulators

To get a good intuition for the topological description of Weyl semimetals, it will be useful to consider a fully insulating material with similar properties first. That is, suppose we have a three-dimensional material that is not subject to any additional symmetries. Such a material is called a 3D Chern insulator, in analogy to the 2D Chern insulator studied in Section 2.3.2.This is not a semimetallic phase in the sense that there are no band crossings in the bulk; still, in some sense it can be considered a limiting case of a Weyl semimetal, where the number of Weyl points is zero.

From the Atland–Zirnbauer classification in Table [reference],one might expect a 3D Chern insulator to be topologically trivial. However, as seen before in equation [reference] (and perhaps also in 3D BHZ/Kane–Mele if I discuss this in ch. 2),the full topological classification of materials depends not only on the top-dimensional topology, but also on that borrowed from lower-dimensional subspaces. In the case of a 3D Chern insulator, this topology arises on two-dimensional slices of the Brillouin zone; an example of such a slice is highlighted in Figure 3.1.

There are three topologically distinct ways to slice up the three-torus, all perpendicular to one of the three coordinate directions.* These slices have the topology of a two-torus $\mathbb{T}^2$, and a Chern number can be obtained by integrating the Berry curvature $\mathcal{F}$ of the system over them: for example, perpendicular to the x direction we obtain $C_x = \int_{\mathbb{T}^2_{yz}} \mathcal{F}$.† This results in a classification by three distinct Chern numbers C_x, C_y and C_z, and in

*Other 2D slices exist, such as those going diagonally across, but these can all be considered linear combinations of the three "orthogonal" slices. To be precise, the different classes of 2D subspaces of $\mathbb{T}^3$ form the second homology group $H_2(\mathbb{T}^3) \cong \mathbb{Z}^3$, and this group is *generated* by the orthogonal slices.

†Note that it does not matter where along the Brillouin zone this yz-slice is taken: the Chern number is an integer, while the system is continuous. This means the x coordinate can be changed continuously without changing the resulting Chern number.

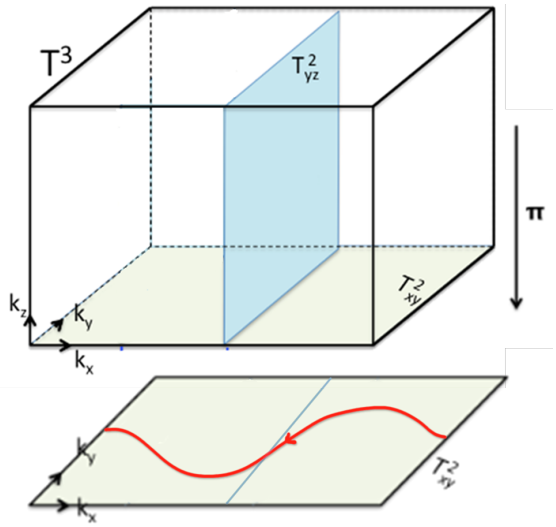

Figure 3.1: [Temporary figure] Three-dimensional Brillouin torus $\mathbb{T}^3$ of a Chern insulator, with a two-dimensional slice $\mathbb{T}^2_{yz}$ indicated in blue. A projection onto a surface Brillouin zone in the xy-direction is also shown, with an example Fermi loop of gapless states in red. In this example, the slice $\mathbb{T}^2_{yz}$ has a Chern number of $C_x = 1$, and so its projection onto the surface is a 1D loop that features one band crossing. Figure adapted from [MT17].

the literature (e.g. [Van18; Liu+22]) these are commonly arranged in a so-called *Chern vector*

$$\mathbf{C} = \begin{pmatrix} C_x \\ C_y \\ C_z \end{pmatrix} \in \mathbb{Z}^3.$$

Importantly, these three Chern numbers are all induced by a single two-form $\mathcal{F}$. In this sense, there is an exact correspondence between topologically distinct Berry curvatures $\mathcal{F}$ and Chern vectors $\mathbf{C} \in \mathbb{Z}^3$. This is precisely what motivates the use of cohomology for classification: just like in the 2D Chern insulator, the two-form $\mathcal{F}$ can be considered to represent a class in the second cohomology group:

$$[\mathcal{F}] \in H^2(\mathbb{T}^3) \cong \mathbb{Z}^3. \tag{3.1}$$

As a result, this group precisely classifies the distinct topological phases of the system.[‡]

Boundary states

Before moving on to a system with Weyl points, it will be instructive to study the gapless modes that arise on the surface of a 3D Chern insulator with non-zero Chern

[‡]More fundamentally, a complex vector bundle called the *valence bundle* can be associated to a gapped Hamiltonian, and the second cohomology group classifies the different complex vector bundles over a manifold.

vector. Figure 3.1 illustrates the case where $\mathbf{C} = (1, 0, 0)^\mathsf{T}$. In this case, $\mathbb{T}^2_{yz}$ is the only orthogonal slice with a non-zero Chern number, and as such the material lattice can be thought of as a stack of 2D Chern insulators spanning the y and z directions, stacked together in the x direction. $\mathbb{T}^2_{yz}$ can effectively be considered the Brillouin zone of such a 2D Chern insulator.

Recall from our discussion in Section 2.3.2 that a 2D Chern insulator with a Chern number of 1 has a single chiral edge mode, which manifests as a gapless state on the one-dimensional surface Brillouin zone. This logic can be translated to the the three-dimensional case, where such slices are stacked in the x direction. Suppose there is a projection π along the z direction, onto a two-dimensional surface Brillouin zone $\widetilde{\mathbb{T}}^2_{xy}$. Then the two-dimensional slices $\mathbb{T}^2_{yz}$ project down to a one-dimensional loop $\pi(\mathbb{T}^2_{yz}) \cong S^1$ containing a single point-like gapless state. As the $\mathbb{T}^2_{yz}$ slice is moved around in the x direction, this band crossing point moves continuously along the y direction, by continuity of the Hamiltonian. It follows that the full two-dimensional surface Brillouin zone must contain a loop of gapless states going across the x direction, as depicted in the figure. This loop is called a Fermi loop, in analogy with the Fermi arcs in a Weyl semimetal, and the existence of such loops is experimentally well documented [references]. Moreover, the chirality of the edge modes can be used to assign a consistent orientation to this loop.

Fermi loops admit a natural topological description in terms of homology. Being oriented loops, they precisely represent a class in the first homology group $H_1(\widetilde{\mathbb{T}}^2)$ of the surface Brillouin zone. Furthermore, it is possible to define an oriented *Dirac loop* ℓ in the bulk Brillouin zone in such a way that its projection $\pi(\ell)$ onto the surface in any direction is exactly the Fermi loop. This loop ℓ represents a first homology class in the bulk Brillouin zone,

$$[\ell] \in H_1(\mathbb{T}^3) \cong \mathbb{Z}^3.$$

It is not a coincidence that this first homology group is isomorphic to the second cohomology group $H^2(\mathbb{T}^3)$ from Equation (3.1). This equivalence is a result of *Poincaré duality*, which is the statement that for any closed oriented d-dimensional manifold M, the isomorphism

$$H_n(M) \cong H^{d-n}(M)$$

holds for any integer n. In the present case, this duality can be stated intuitively in terms of Chern numbers, which count the number of signed intersections of the Dirac loop with the different two-dimensional slices of the Brillouin zone. This duality can be summarised schematically as follows:

$$H^2(\mathbb{T}^3) \ni [\mathcal{F}] \overset{\text{integration}}{\Longleftrightarrow} \mathbf{C} \overset{\text{intersections}}{\Longleftrightarrow} [\ell] \in H_1(\mathbb{T}^3).$$

This Poincaré duality ensures that the classifications in terms of first homology and second cohomology are completely equivalent in this case. Importantly, however, Poincaré duality depends on orientability, and it will not hold when we consider non-orientable Brillouin zones in the next chapter. As such, the question of which group provides the right classification of such a system will be key. For the moment, we turn our attention to the topology of Weyl points in the simpler orientable setting.

3.2.2 Introducing Weyl points

Consider a Weyl semimetal with a set of k Weyl points

$$W \equiv \{ w_1, w_2, \ldots, w_k \} \subset \mathbb{T}^3.$$

Then the charge of a Weyl point w_i is given by the Chern number

$$C_w = \int_{S_w^2} \mathcal{F}, \tag{3.2}$$

where S_w^2 is a sufficiently small 2-sphere centred at w—in particular, it must be small enough to contain no other Weyl points in its interior. The Nielsen–Ninomiya charge cancellation theorem is the statement that all these charges must add to zero:

$$\sum_{i=1}^{k} C_{w_i} = 0. \tag{3.3}$$

This cancellation can be demonstrated using Stokes' theorem. The argument goes as follows: imagine the small open 3-ball bounded by S_w^2 is removed from $\mathbb{T}^3$ around each Weyl point w. The resulting 3-manifold X looks like a 3-torus with small holes, and its boundary is given by the collection of 2-spheres around the Weyl points:

$$\partial X = -\bigcup_{i=1}^{k} S_{w_i}^2,$$

where the minus sign induces the correct orientation. Then Stokes' theorem gives

$$0 = \int_{\partial X} \mathrm{d}\mathcal{F} = -\sum_{i=1}^{k} \int_{S_{w_i}^2} \mathcal{F} = -\sum_{i=1}^{k} C_{w_i}.$$

A similar argument can also be applied to study what happens to Chern numbers on two-dimensional slices of the Brillouin zone when Weyl points are introduced. This argument is illustrated in Figure 3.2. Here two slices $\mathbb{T}_L^2$ and $\mathbb{T}_R^2$ are placed on either side of a Weyl point w with charge $C_w = q$, along with a small sphere S_w^2 surrounding it. These spaces then bound a three-dimensional manifold Y as indicated in the figure, given the following orientations:

$$\partial Y = \mathbb{T}_R^2 - \mathbb{T}_L^2 - S_w^2.$$

The same Stokes' theorem argument can then be used to relate the Chern numbers C_L and C_R on the respective slices, yielding

$$C_R = C_L + C_w = C_L + q.$$

That is, the Chern number of a two-dimensional slice increases by q every time it passes over a Weyl point with charge q. As a sanity check, it should be noted that this process

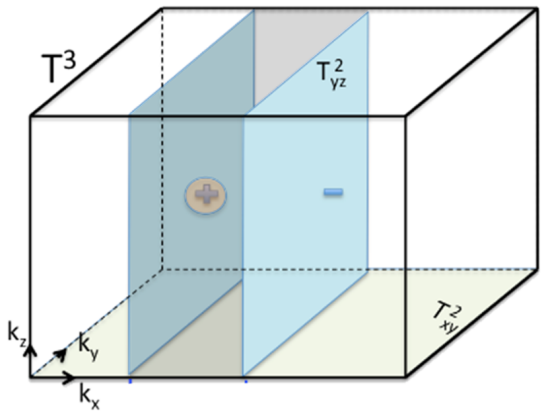

Figure 3.2: Brillouin torus $\mathbb{T}^3$ of a Weyl semimetal with two oppositely charged Weyl points labelled + and −. Three two-dimensional subspaces are indicated in blue: a yz-like 2-torus on either side of the + point, and a small 2-sphere surrounding it. Given the proper orientation, the blue spaces form the boundary of a three-dimensional manifold Y, shaded in grey here. Figure from [MT17]. [not yet licensed; may need better labelling]

respects the periodicity of the Brillouin torus: indeed, when the slice is passed over the entire torus, charge cancellation ensures that the added Chern number is zero in total.

All in all, the presence of Weyl points allows for a finer collection of Chern numbers to appear in the Brillouin zone, beyond the $\mathbb{Z}^3$ Chern vector of the insulating case. This behaviour can be captured using cohomology. The key idea is that the Berry curvature can only be integrated over subspaces where the gap never closes, so that the set of Weyl points W needs to be excluded. To be precise, we are interested in classifying possible Chern numbers on $\mathbb{T}^3 \setminus W$, the Brillouin zone minus W; these correspond precisely to all possible gapless phases on $\mathbb{T}^3 \setminus W$. This means the Berry curvature now lives in the second cohomology group of this space:

$$[\mathcal{F}] \in H^2(\mathbb{T}^3 \setminus W) \cong \mathbb{Z}^3 \oplus \mathbb{Z}^{k-1}, \tag{3.4}$$

where k again is the number of Weyl points. It follows that there are $k-1$ extra factors of $\mathbb{Z}$ involved in the classification of a Weyl semimetal compared to that of a 3D Chern insulator. One might expect this to be k factors, but the reduction by one is a natural result of Nielsen–Ninomiya: for example, if $k = 1$ then charge cancellation implies that the single Weyl point must have a charge of 0, and so it is not topologically protected.

Fermi arcs

The varying Chern numbers over Weyl points help explain how Fermi arcs arise on the surface. As discussed in the case of a 3D Chern insulator, Fermi loops on the surface arise whenever there is a non-zero Chern number in some direction. Similarly, Fermi arcs

begin and terminate whenever the presence of a Weyl point causes a change in the Chern number; this is illustrated in Figure 3.3.

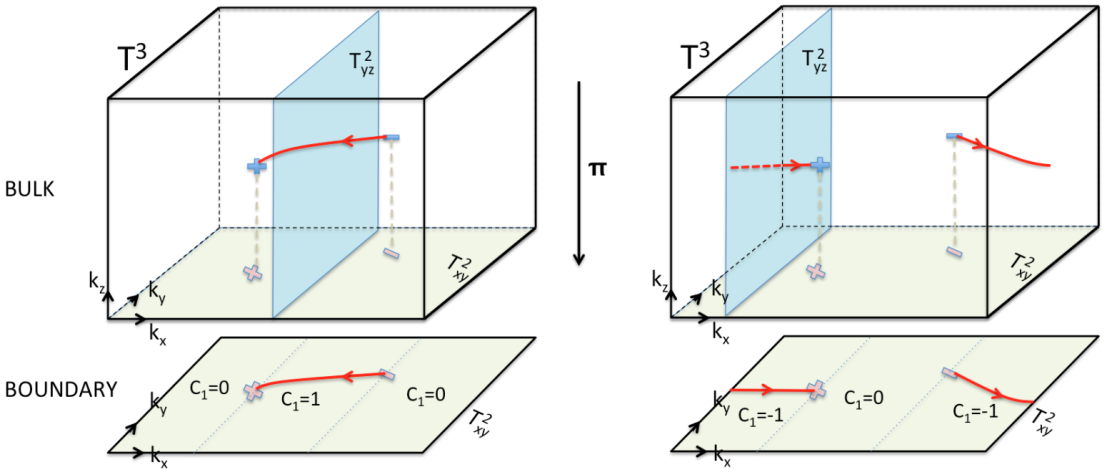

Figure 3.3: Two semimetal Brillouin zones are shown with the same configuration of Weyl points, but featuring topologically distinct Fermi arcs (shown in red on the boundary). The distinction is due to different bulk Chern numbers: Fermi arcs appear in regions where the bulk Chern number is non-zero. These Fermi arcs can be considered to be the projection of a Dirac string (shown in red in the bulk). Figure from [MT17].

3.2.3 The Mayer–Vietoris sequence

Chapter 4

Non-orientable manifolds

4.1 Mathematical exploration

Concepts explored in personal notes so far:

- Calculations of (co)homology and semimetal MV sequence for manifolds in ≥ 2 dimensions:
  - All compact surfaces without boundary, i.e. the surfaces M_g and N_g
  - All spaces of the form $M = K^2 \times \mathbb{T}^{d-2}$
- The map $\Sigma : H^{d-1}(\bigsqcup_k S^{d-1}) \to H^d(M)$ in the semimetal MV has a clear interpretation in terms of total charge in the (orientable) $d = 3$ case. This would provide a clear picture of the total charge cancellation in the orientable case ($H^d(M) = \mathbb{Z}$ in general) vs. the mod 2 charge cancellation in the non-orientable case ($H^d(M) = \mathbb{Z}_2$ in general).
- However, Σ and the other maps in the MV sequence are difficult to interpret in the $\chi \neq 0$ case (maybe even generally for odd dimensions). Taking the oriented case as an example, the MV sequence ends as

$$H^{d-1}(M \setminus \Delta) \;\to\; H^{d-1}\left(\bigsqcup_k S^{d-1}\right) \cong \mathbb{Z}^k \;\xrightarrow{\Sigma}\; H^d(M) \cong \mathbb{Z}$$

  so that the "charge configuration" in $\mathbb{Z}^k$ must map to 0 by Σ in order to descend from the semimetal, regardless of whether $\chi = 0$.
- This may imply that the Bloch vector field carries more topological information about the total charge than the MV sequence (which makes sense since it generates *all* homology groups of the valence bundle, and all Betti numbers factor into χ). As a concrete example, consider $M = S^2$ with a single puncture of charge $+2$. The punctured sphere is topologically a disc, so that the valence bundle must be trivial, while the Bloch vector field is topologically non-trivial in the sense that it has an

index +2 singularity. In addition, all relevant $H_n(A) \oplus H_n(B)$ are zero, so that the semimetal MV reduces to the statement that $H_2(S^2) \cong H_1(S^1)$.

- It may even be the case that the valence bundle cannot be generated from the Bloch vector field in the $d = 2$ case; it's probably worth studying the $d \in \{3, 4, 5\}$ cases (pullback of some universal bundle) to learn more about this. The $d = 3$ case should be especially helpful in understanding how the valence bundle arises from the vector field.

- A complicating factor in the non-orientable case is that the homology groups are different from the cohomology groups, since the torsion moves up one dimension. This makes the homological semimetal MV different from the cohomological one (it's a short exact sequence in $d \geq 3$!), and this leads to additional challenges in interpretation.

- The map $H : \mathbb{R}^3 \to \mathfrak{su}(2)$, $\vec{h} \mapsto \vec{h} \cdot \vec{\sigma}$ is an isomorphism of Lie algebras, with the cross product as a Lie bracket on $\mathbb{R}^3$. Still the vector field is discontinuous on a non-orientable manifold, while H is not. This suggests an alternative approach for constructing the valence bundle: consider h as a map $M \to \mathbb{R}^d$ instead of an element of $\mathfrak{X}(M)$, and then pull back the universal bundle along the unit map $\hat{h} : M \setminus \Delta \to S^{d-1}$. That is, we detach $\vec{h}$ from the tangent bundle and consider it a more abstract map. An added "benefit" of this is that we lose all coordinate dependence. However, this may also be a downside in the sense that the map will not be subject to the same constraints (Poincaré–Hopf etc.) that the vector field is; for example, $S^2 \to \mathbb{R}^2$, $x \mapsto (1, 0)$ is a perfectly valid map that would violate the hairy ball theorem as a vector field (and this is a result of being unable to cover S^2 by a single chart). At this point the question may become more about which description is more physical in nature, and the non-orientable Weyl point paper[Fon+24] seems to imply there may be more to the $h : M \to \mathbb{R}^3$ story. It also seems to agree better with the intuition of an applied external potential removing all Weyl nodes – something that's impossible for $\chi \neq 0$ if charge corresponds to vector field index. It also explains how the valence bundle can be trivial on the once punctured S^2.

- In light of the previous point, this may be an important observation: every d-manifold M with $\chi(M) = 0$ admits a nowhere-vanishing vector field (link). ~~This may imply that the vector field description is equivalent to the map to $\mathbb{R}^d$ in these cases, though one needs to be careful about charts. It would be good to find or write a (dis)proof for something like $\mathfrak{X}(M) \cong C^\infty(M, \mathbb{R}^d)$ (or similar for non-vanishing maps) in this case. Or more specifically:~~

$$~~\left[M \setminus \Delta, S^{d-1}\right] \overset{?}{\cong} \left\{ \vec{h} \in \mathfrak{X}(M \setminus \Delta) \,\middle|\, \vec{h} \text{ is non-vanishing} \right\}~~$$

Update: I think the real requirement for equivalence is that the base manifold M is parallelisable (i.e. has a trivial tangent bundle), since we're essentially using a trivial $\mathbb{R}^d$-bundle in this construction.

- Any smooth d-manifold can be given a CW complex structure with one d-cell (link). On this d-cell there is an exact correspondence between vector fields and maps to $\mathbb{R}^d$, since it can be embedded in $\mathbb{R}^d$. What distinguishes the two is how points on the boundary of the d-cell are identified with each other; this determines whether the "vectors" need to change orientation. To illustrate:

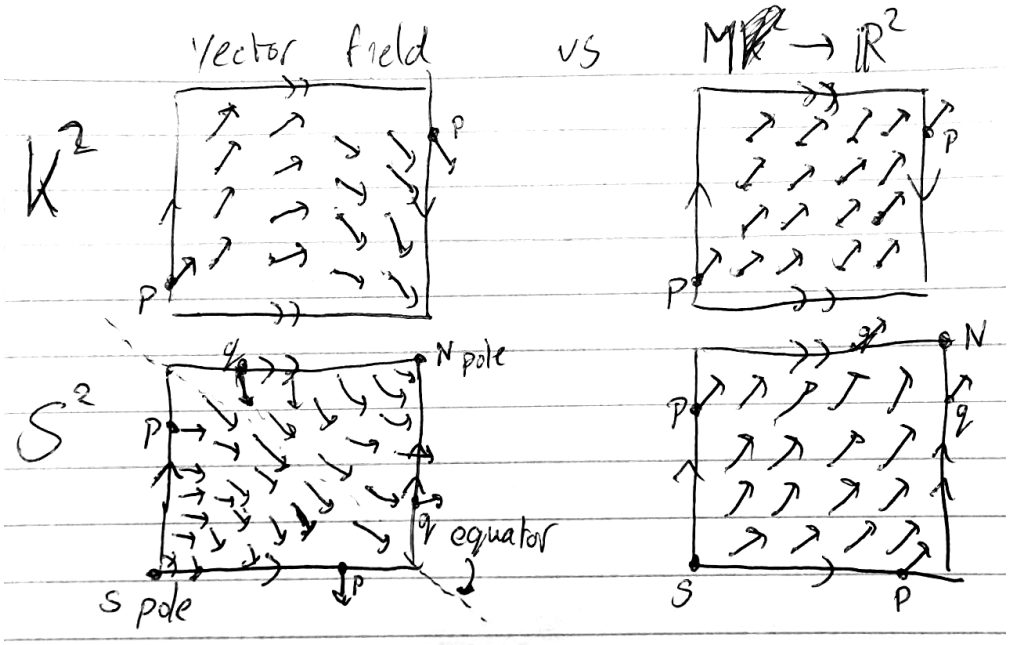

- On any orientable manifold, the Stokes' theorem argument shows that the total charge must be zero regardless of Euler characteristic:

$$\sum_\alpha w(S_\alpha) = \sum_\alpha \int_{S_\alpha} c_1(E) = \sum_\alpha \int_{S_\alpha} \frac{\operatorname{Tr} \mathcal{F}}{2\pi} = \int_{B'} \mathrm{d} \frac{\operatorname{Tr} \mathcal{F}}{2\pi} = 0$$

  where the last equality holds by the Bianchi identity for the trace. This means the valence bundle cannot be a pullback along a tangent vector field for $\chi \neq 0$.

  On a non-orientable manifold, this argument doesn't hold since the integral over B' isn't well defined.

- Total chirality isn't well defined on a non-orientable manifold (at least in odd dimensions, not sure how to interpret even dimensions). Still there is charge cancellation in the form of Fermi arcs etc.; it may take moving to a different homology system to get the full picture, such as homology with local coefficients or equivariant homology. (See e.g. [TSG17])

- It may be worth classifying which manifolds are candidates for physical material Brillouin zones; I have a feeling that this might be restricted to those manifolds for which the n-torus is a covering space. In this case a full classification of symmetries

on the torus (and e.g. their related equivariant homologies) would be sufficient to classify all material topologies.

4.2 Physical implications

Appendix A

Homology and cohomology

The concepts of homology and its counterpart cohomology are indispensable in algebraic topology.

Here we offer a brief introduction to these concepts, aimed at the uninitiated physicist. The goal here is not to be completely rigorous, but to give a sufficiently complete understanding that the applications discussed in the main text may be understood in their proper context. For a more complete picture, the interested reader is referred to standard texts in algebraic topology such as [Hat02] and [Bre93]. A more geometric treatment is also found in [BT82].

A.1 Homotopy

A.2 Homology

Suppose we have some topological space—for example, the torus $\mathbb{T}^2$—and we want to study

The basic idea underlying homology is that information about the topology of a space can be gained from studying non-trivial subspaces. In the related *homotopy* theory, this is achieved by mapping n-dimensional spheres into the space, and seeing whether or not they can be contracted to a point.

A.3 Cohomology

Bibliography

[Akh+] Anton Akhmerov et al. *Online course on topology in condensed matter*. URL: https://topocondmat.org/ (visited on 10/07/2024).

[AOP16] János K. Asbóth, László Oroszlány, and András Pályi. *A Short Course on Topological Insulators*. Springer International Publishing, 2016. ISBN: 9783319256078. DOI: 10.1007/978-3-319-25607-8. URL: http://dx.doi.org/10.1007/978-3-319-25607-8.

[Ata+13] Marcos Atala et al. "Direct measurement of the Zak phase in topological Bloch bands". In: *Nature Physics* 9.12 (Nov. 2013), pp. 795–800. ISSN: 1745-2481. DOI: 10.1038/nphys2790. URL: http://dx.doi.org/10.1038/nphys2790.

[BH13] B. Andrei Bernevig and Taylor L. Hughes. *Topological insulators and topological superconductors*. Princeton University Press, 2013. ISBN: 978-0-691-15175-5.

[Blo29] Felix Bloch. "Über die Quantenmechanik der Elektronen in kristallgittern". In: *Zeitschrift für Physik* 52.7–8 (July 1929), pp. 555–600. DOI: 10.1007/bf01339455.

[Bre93] Glen E. Bredon. *Topology and geometry*. 139. Springer International Publishing, 1993. ISBN: 978-1-4419-3103-0. DOI: 10.1007/978-1-4757-6848-0.

[BT82] Raoul Bott and Loring W. Tu. *Differential Forms in Algebraic Topology*. 82. New York, NY: Springer Science+Business Media New York, 1982. ISBN: 978-1-4419-2815-3. DOI: 10.1007/978-1-4757-3951-0.

[Fon+24] André Grossi Fonseca et al. "Weyl Points on Nonorientable Manifolds". In: *Phys. Rev. Lett.* 132 (26 June 2024), p. 266601. DOI: 10.1103/PhysRevLett.132.266601. URL: https://link.aps.org/doi/10.1103/PhysRevLett.132.266601.

[Fre+04] Michael Freedman et al. "A class of P,T-invariant topological phases of interacting electrons". In: *Annals of Physics* 310.2 (2004), pp. 428–492. ISSN: 0003-4916. DOI: https://doi.org/10.1016/j.aop.2004.01.006. URL: https://www.sciencedirect.com/science/article/pii/S0003491604000260.

[Geh+13] P. Gehring et al. "A Natural Topological Insulator". In: *Nano Letters* 13.3 (Mar. 2013), pp. 1179–1184. ISSN: 1530-6992. DOI: 10.1021/nl304583m. URL: http://dx.doi.org/10.1021/nl304583m.

[Hat02] Allen Hatcher. *Algebraic Topology*. Cambridge: Cambridge Univ. Press, 2002. URL: https://pi.math.cornell.edu/~hatcher/AT/ATpage.html (visited on 10/07/2024).

[Liu+22] Gui-Geng Liu et al. "Topological Chern vectors in three-dimensional photonic crystals". In: *Nature* 609 (2022), pp. 925–930. DOI: 10.1038/s41586-022-05077-2.

[MAG16] Eric J Meier, Fangzhao Alex An, and Bryce Gadway. "Observation of the topological soliton state in the Su–Schrieffer–Heeger model". en. In: *Nat. Commun.* 7.1 (Dec. 2016), p. 13986.

[MT17] Varghese Mathai and Guo Chuan Thiang. "Differential Topology of Semimetals". In: *Communications in Mathematical Physics* 355.2 (July 2017), pp. 561–602. ISSN: 1432-0916. DOI: 10.1007/s00220-017-2965-z. URL: http://dx.doi.org/10.1007/s00220-017-2965-z.

[SA17] Masatoshi Sato and Yoichi Ando. "Topological superconductors: a review". In: *Reports on Progress in Physics* 80.7 (May 2017), p. 076501. ISSN: 1361-6633. DOI: 10.1088/1361-6633/aa6ac7. URL: http://dx.doi.org/10.1088/1361-6633/aa6ac7.

[SSH79] W. P. Su, J. R. Schrieffer, and A. J. Heeger. "Solitons in Polyacetylene". In: *Phys. Rev. Lett.* 42 (25 June 1979), pp. 1698–1701. DOI: 10.1103/PhysRevLett.42.1698. URL: https://link.aps.org/doi/10.1103/PhysRevLett.42.1698.

[SSH80] W. P. Su, J. R. Schrieffer, and A. J. Heeger. "Soliton excitations in polyacetylene". In: *Phys. Rev. B* 22 (4 Aug. 1980), pp. 2099–2111. DOI: 10.1103/PhysRevB.22.2099. URL: https://link.aps.org/doi/10.1103/PhysRevB.22.2099.

[TSG17] Guo Chuan Thiang, Koji Sato, and Kiyonori Gomi. "Fu–Kane–Mele monopoles in semimetals". In: *Nuclear Physics B* 923 (Oct. 2017), pp. 107–125. ISSN: 0550-3213. DOI: 10.1016/j.nuclphysb.2017.07.018. URL: http://dx.doi.org/10.1016/j.nuclphysb.2017.07.018.

[Van18] David Vanderbilt. *Berry Phases in Electronic Structure Theory: Electric Polarization, Orbital Magnetization and Topological Insulators*. Cambridge University Press, 2018, pp. 215–218. DOI: https://doi.org/10.1017/9781316662205.